

Research article

Shape memory properties of polyamide/thermoplastic polyurethane films and sea-island fibers

Cheng-Chieh Chang, Chang-Mou Wu*, Kei-Chieh Chang

Department of Materials Science and Engineering National Taiwan University of Science and Technology, 10607 Taipei, Taiwan, Republic of China

Received 6 December 2024; accepted in revised form 14 March 2025

Abstract. In this study, polyamide 11/thermoplastic polyurethane thermally responsive shape-memory composite fibers were fabricated using a bi-component melt-spinning machine with a sea-island spinning nozzle. Polyamide 11, a material with low water absorption and good oil resistance, was used as the ‘sea’, whereas the thermoplastic elastomer was used as the ‘island’ to provide shape memory performance.

A film was prepared from these materials, and its suitability for preparing the fibers was determined using its shape memory behavior. The results demonstrated that the shape memory of the film fixation rate was 99.6% and the recovery rate was 92.3%, proving that polyamide 11/polyurea (PA11/PUA) has good shape memory fixation and recovery rates. During the melt-spinning and take-up processes, the as-spun fiber was collected into a roll with a certain draw ratio, resulting in a better molecular orientation and, consequently, an improved shape memory effect. After three shape memory cycles, the fixation rate of the PA11/PUA fiber was 98.8%, and the recovery rate was 99.9%. Thus, sea-island shape memory composite fibers were successfully produced, and are expected to enable shape memory materials to find a wider range of applications.

Keywords: mechanical and shape memory properties, polyamide 11, thermoplastic polyurethane, sea-island fiber

1. Introduction

Shape memory polymers (SMP) are a type of functional material that deform under external stimuli and have seen gradual development since 1980. SMP fibers exhibit complex and controllable shape-changing behaviors, superior mechanical properties, superior recovery stress, and excellent design abilities. Therefore, SMP fibers have been widely used to fabricate shape-memory composites for flexible sensors and actuators, self-healing materials, smart textiles, and smart structures [1–6].

SMPs have unique permanent network structures (chemical or physical cross-links) as fixing phases and reversible switch phases (amorphous or crystalline) that memorize their temporary shapes. Traditional thermally induced shape memory polymers

are multiblock copolymers composed of soft and hard segments. The hard segments act as physical cross-linking points that maintain the permanent shape of the material. The soft segment temporarily fixes the shape of the material via crystallization or glass transition. Triple and multi-SMPs based on copolymers or polymer blends have been developed to achieve two or more temporary shape changes [7–11]. Modifying polyamides by melt blending has been well documented in the literature [11–19]. Rashmi *et al.* [20], were the first to blend polyamide-11 (PA11) with thermoplastic polyurethane (TPU) to create bio-alloys and investigate their shape memory behavior. Their results revealed strong hydrogen bonding between the two materials, with TPU effectively toughening PA11. However, polyurea

*Corresponding author, e-mail: cmwu@mail.ntust.edu.tw
© BME-PT

(PUA) has more N-H bonds than thermoplastic polyurethane (TPU); hence, it would need to exhibit higher compatibility to observe its influence on shape memory. In this study, bicomponent melt-spinning was used to produce shape memory fibers, and polyamide 11 (PA11)/PUA sea-island composite fibers were successfully prepared. These shape memory fibers can be processed into functional textiles through postprocessing.

2. Experiment

2.1. Materials

Polyamide 11 (Arkema RILSAN® BMNO P40 TLD) was purchased from Arkema Company Limited Taiwan Branch. Polyurea (PUA, TY-98) was obtained from Coating P. Materials Co., Ltd.

2.2. Preparation of PA11/PUA film

The PA11 and PUA masterbatches were dried at 100 °C in a vacuum oven for 4 h to remove any excess moisture. The samples were then crushed using a high-speed grinder. Finally, the resultant PA11 and PUA powders were placed in a hot press (NTUST, Buquan Industrial, Taiwan) in a weight ratio of 1:1. They were maintained at 220 °C for 1 min with a pressure of 1.5 MPa to prepare a PA11/PUA film with a thickness of 0.25 mm.

2.3. Preparation of PA11/PUA composite fiber

The PA11 and PUA masterbatches were dried at 80 °C in a vacuum oven for 24 h to remove any excess

moisture. The melt flow indices of PA11 and PUA were 38 g/10 min and 26 g/10 min at 220 °C (2.16 kg), respectively. A bicomponent melt-spinning machine (NTUST, Together Plastic Chemical Power Company, Taiwan) with a sea-island spinning nozzle (Figure 1) was used to prepare the PA11/PUA sea-island-type composite fibers. The die temperature was 220 °C; the chamber temperature was 205–215 °C; the extrusion rate was 26–30 rpm; and take-up speeds were 220, 205–215, 26–30, and 800 m/min.

2.4. Characterization methods

Cross-linking density

The cross-linking density was determined by equilibrium swelling [21, 22]. Swelling experiments were conducted with cured samples by immersing the samples in toluene at 65 °C for 24 h to achieve equilibrium swelling. The solvent uptake percentage Q and volume fraction of the film (or fiber) in the swollen gel V_r were calculated using the Equations (1)–(3):

$$Q = \frac{m_2 - m_1}{m_1} \quad (1)$$

$$V_r = \frac{\frac{1}{\rho_{\text{sam}}}}{\frac{1}{\rho_{\text{sam}}} + \frac{\rho}{\rho_{\text{sol}}}} \quad (2)$$

$$\nu = -\frac{\ln(1 - V_r) + V_r + \chi V_r^2}{V_{\text{sol}} \left(V_r^{1/3} - \frac{V_r}{2} \right)} \quad (3)$$

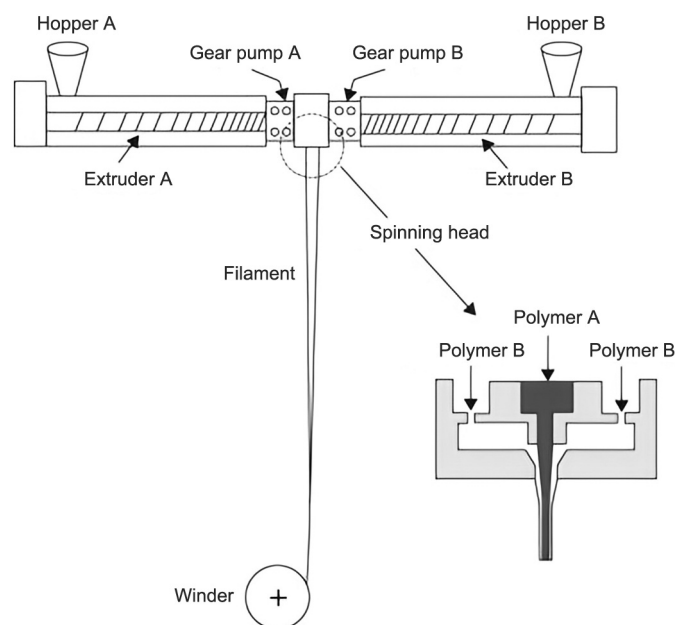


Figure 1. Schematic diagram of a bi-component melt spinning machine.

where m_1 and m_2 are the weights of the film (or fiber) sample before immersion in the solvent and in the swollen state, respectively.

ρ_{sam} and ρ_{sol} are the densities of the sample and the solvent. V_{sol} is the molar volume of the swelling solvent (106 cm³/mole in toluene). χ is the Flory-Huggins (sample-toluene) interaction parameter and was considered as 0.1995 in this calculation [21, 22].

The cross-linking density of the sample ν , defined by the number of elastically active chains per unit volume, was calculated by the Flory-Rehner equation [23], which is expressed in Equation (3).

Shape memory measurement method

Shape memory properties can be described by strain–temperature–stress curves. The shape fixation rate (R_f) and shape recovery rate (R_r) were measured under free-recovery conditions, and shape recovery stress was measured under constrained recovery conditions [24]. This study was conducted in accordance with the test methods described in references [25, 26]. These strain parameters are substituted into Equations (4) and (5) to calculate the fixed and recovery rates of the materials, respectively:

$$R_f = \frac{\epsilon_x}{\epsilon_{x,\text{load}}} \quad (4)$$

$$R_r = \frac{\epsilon_x - \epsilon_{y,\text{rec}}}{\epsilon_x - \epsilon_y} \quad (5)$$

where ϵ_x is the strain after the removal of the stress, $\epsilon_{x,\text{load}}$ is the applied strain, $\epsilon_{y,\text{rec}}$ (measured after the cooling step) is the maximum strain obtained in the sample and ϵ_y is the residual strain after the recovery. In constrained recovery experiments, the bottom grip was released to ensure zero load at the beginning of the recovery step. The bottom of the specimen was re-gripped before the recovery process was initiated. This gripping procedure results in a compressive force acting on the SMP. At the end of the recovery heating, the samples were held for 15 min at 70 °C, following which the thermomechanical cycle was repeated.

Fourier-transform infrared spectroscopy

The chemical structures of the samples were investigated using Fourier-transform infrared spectroscopy in attenuated total reflectance mode (ATR-FTIR, FTIR 6800 JASCO, Tokyo, Japan).

Polarized optical microscopy

Film morphologies were investigated using a polarized optical microscope (POM, BHZ-UMA, Olympus, Japan) equipped with a hot stage (TMS 600 and CCD SG-3200). A phase-separation test piece was prepared by placing a small amount of mixed powder between two circular sheets with a diameter of 17 mm and a thickness of 0.1 mm. After the sheets melted, pressure was applied to reduce their thicknesses. After the sheets melted, they were cooled to a heated water-cooled stage. The two-phase distribution, crystallization, and microstructure were observed under a polarizing microscope in light source penetration mode.

Differential scanning calorimetry

The thermal behaviors of the samples were investigated using differential scanning calorimetry (DSC, DSC 6000, PerkinElmer, USA). First, the temperature was increased from 30 to 250 °C at a heating rate of 20 °C/min, and then cooled to 0 °C at a cooling rate of 5 °C/min to eliminate the thermal history of the material. Subsequently, the temperature was increased to 250 °C at a heating rate of 5 °C/min. The melting point and recrystallization temperature of the material were determined from the DSC curve.

Dynamic mechanical analysis

The glass transition temperature (T_g) was determined by dynamic mechanical analysis (DMA, DMA Q800, TA Instruments, USA). The film was cut into 25×7×0.55 mm for testing, and 25 mm was used for the initial spinning fiber test. The parameters were as follows: frequency 1 Hz, amplitude 10 μm, pre-stress 0.01 N, temperature increased from –100 to 120 °C, heating rate 3 °C/min, and clamp spacing 12 mm. The ratio of the loss modulus to the storage modulus is defined as $\tan\delta$, and the peak value of $\tan\delta$ represents the glass transition temperature of the material.

Mechanical characterization

The mechanical properties of the original and healed samples were studied using a tensile-testing machine (QC-508M2, Comtech Testing Machines, Taiwan).

3. Results and discussion

3.1. FTIR Analysis

Figure 2 shows that PUA has two –NH₂ vibration peaks at 3300 and 1630 cm^{–1} and a –C=O vibration

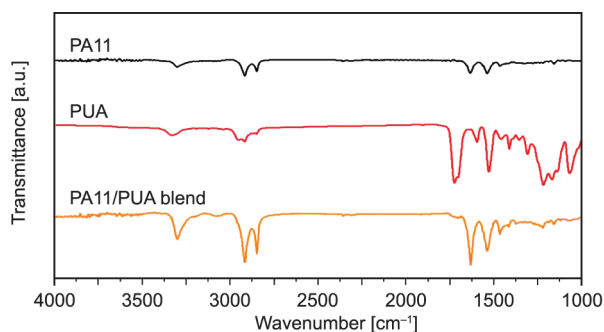


Figure 2. FTIR spectra of PA11, PUA, and the PA11/PUA blend. The -NH_2 vibration peaks of PUA are at 3300 and 1630 cm^{-1} , and the -C=O vibration peak is at 1720 cm^{-1} . The -NH_2 vibration peaks of PA11 are at 3300 and 1645 cm^{-1} , and the -CH_2 vibration peaks are at 2850 and 2925 cm^{-1} . After blending, the intensity of the -C=O vibration peak of PUA at 1720 cm^{-1} decreases significantly, proving that hydrogen bonds are generated between the two system.

peak at 1720 cm^{-1} . PA11 showed two -NH_2 vibration peaks at 1645 and 3300 cm^{-1} and -CH_2 vibration peaks at 2850 and 2925 cm^{-1} [27]. As shown in Figure 2, the peak at 1720 cm^{-1} (-C=O vibration) decreased significantly for PA11/PUA, indicating the formation of hydrogen bonds between the urethane groups of PUA and the amide groups of PA11.

3.2. Thermal analysis

The DSC heating curve of PA11/PUA is shown in Figure 3. The melting point of PUA was originally 157°C . After melt blending with PA11, the melting

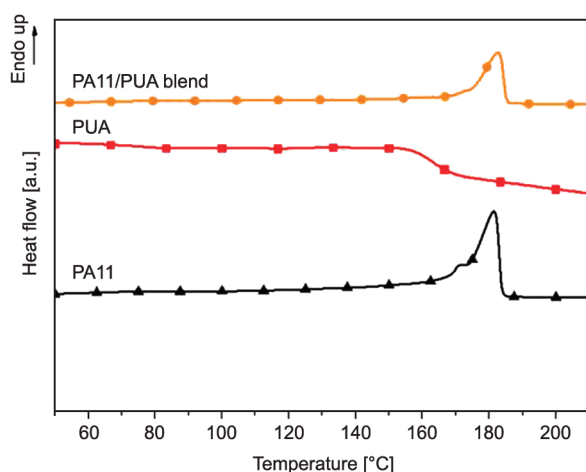


Figure 3. DSC heating curves of PA11, PUA and PA11/PUA blend. The melting points of pure PUA and PA11 are 157°C and approximately 180°C , respectively. After blending with PA11, the melting point of PUA disappears and only the melting point of PA11 remains at approximately 180°C .

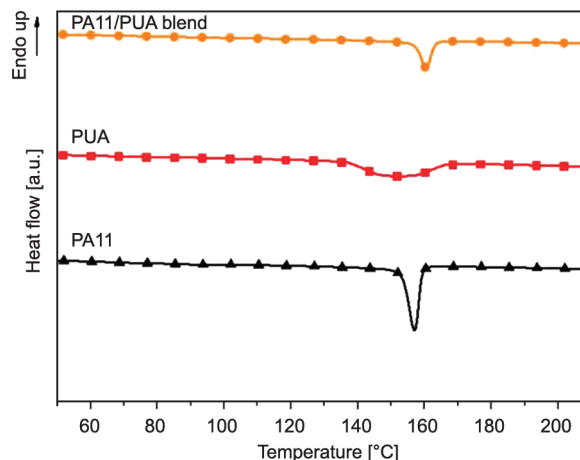


Figure 4. DSC cooling curves of PA11, PUA, and the PA11/PUA blend.

peak of PUA disappeared. The melting peak of PA11 was approximately 180°C . Compared with pure PA11, PA11/PUA exhibited PUA properties, and the phase of the blend changed. The cooling curve of PA11/PUA in Figure 4 shows that the introduction of PUA reduced the crystallization peak area and enthalpy required to decrease and accelerate crystallization.

3.3. Morphological analysis

The blend morphology significantly affected the mechanical properties of the product [29]. The microphase separation of the two systems was observed with a polarizing microscope and a water-cooled hot stage. The test piece was heated to 200°C to make both phases molten, then cooled to room temperature with a $10^\circ\text{C}/\text{min}$ cooling rate. In the PA11/PUA system, PA11 crystallized first. As shown in Figure 5, Figure 5a is in a molten state at 200°C , while Figure 5b is crystalline at 150°C . The DSC cooling crystallization curve suggested that the results correspond to the crystallization of PA11. Figure 5c shows the crystallization conditions of the PA11/PUA test piece at 140°C ; in contrast, Figure 5b shows no further crystallization where preliminary crystallization has occurred. The DSC cooling crystallization curve suggested that PUA crystallized.

In Figure 5d, the POM diagram at room temperature defines the continuous phase structure of PUA as the interpenetrating polymer network (IPN) structure. The PUA system has clear interfaces and interleaves. This IPN structure converts the blend into a cross-network, contributing to the shape memory performance.

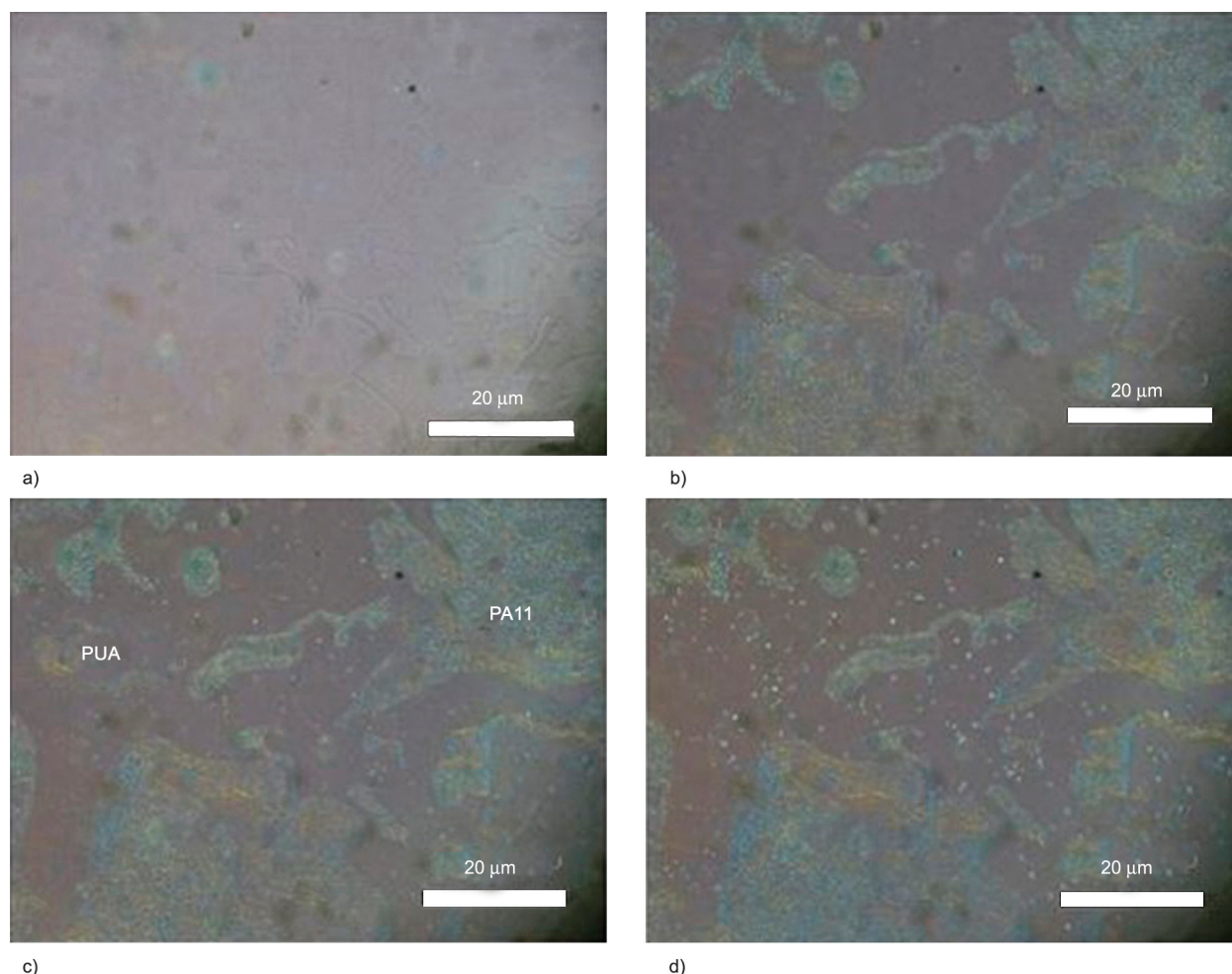


Figure 5. POM micrographs showing the PA11/PUA blend microstructure. All test piece was heated to 200 °C to make both phases molten, then cooled to room temperature with a 10 °C/min cooling rate. a) Results of the PA11/PUA blend at 200 °C (in a molten state); b) results of the PA11/PUA blend after cooling to 150 °C (in a crystalline state). The formation of a crystalline phase was observed and compared with the DSC cooling curve, it was inferred that it was the crystallization of PA11; c) results of the PA11/PUA blend after cooling to 140 °C (in a crystalline state). Compared with Figure 5b these results show no further crystallization where preliminary crystallization has occurred, and from the DSC cooling curve, it was inferred that it was the crystallization of PUA; d) results of the PA11/PUA blend after cooling to room temperature. It can be observed that PA11 and PUA have obvious interfaces and intertwine with each other so that this blend system can be defined as an interpenetrating polymer network (IPN).

3.4. Dynamic viscoelastic property analysis

The peak value shown by PA11 in the DMA curve can be divided into α , β , and γ local motions, as described in the literature [28]. PA11 shows the main α -peak at 53 °C, which is associated with the glass transition. The β -relaxation at 7 °C is water-sensitive and attributed to local motions involving amide bonds. Finally, a low-temperature γ -peak at –80 °C is associated with the local motions of methylene sequences. The dynamic viscoelastic analysis was divided into two parts: film and fiber. The local motion changes of the α , β , and γ -peaks of PA11 were used to explain the peak changes of PA11 and PUA when

melt-blending and spinning the composite fibers, respectively.

Figure 6 shows the two peaks for the pure PUA film. The peak at –87 °C represents the glass transition temperature of the PUA soft segment, and that at –12 °C represents the glass transition temperature of the PUA hard segment. After blending with PA11, the peak for the PA11/PUA film appears at three different temperatures: –72, –28, and 17 °C. The peak at –72 °C corresponds to the γ -relaxation of the PUA soft segment and PA11; the peak at –28 °C is the result of the PA11 β -relaxation being affected by PUA and shifting to a lower temperature; and the peak at

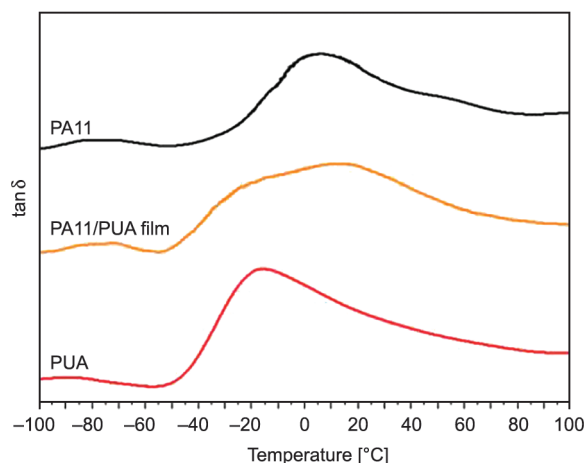


Figure 6. $\tan \delta$ of PA11, PUA, and PA11/PUA film. After blending with PA11, the peak for the PA11/PUA film appears at three different temperatures: -72 , -28 , and 17 °C. The peak at -72 °C corresponds to the γ -relaxation of the PUA soft segment and PA11; the peak at -28 °C is the result of the PA11 β -relaxation being affected by PUA and shifting to a lower temperature; and the peak at 17 °C is the result of the PA11 α -relaxation being affected by PUA and shifting to a lower temperature.

17 °C is the result of the PA11 α -relaxation being affected by PUA and shifting to a lower temperature. Figure 7 shows the $\tan \delta$ characterization of PA11/PUA sea-island composite fibers, with peak values at -20 and 48 °C. The peak at -20 °C is defined as the contribution of the PUA hard segment, and the peak at 48 °C is defined as the β -relaxation contribution of PA11 (Table 1). In contrast with the film system, the PA11/PUA composite fiber did not exhibit the peak value of the PUA soft segment contribution during the $\tan \delta$ test process. It is speculated that this peak was not evident in the fiber system. The T_g determined by $\tan \delta$ is used as the basis to define

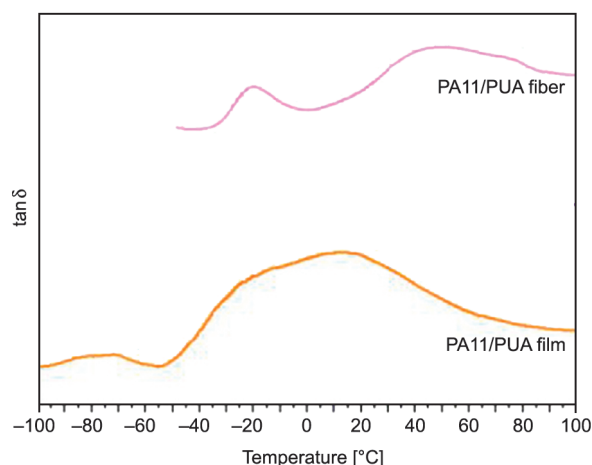


Figure 7. $\tan \delta$ of PA11/PUA film and fiber. In contrast with the film system, the PA11/PUA composite fiber did not exhibit the peak value of the PUA soft segment contribution during the $\tan \delta$ test process.

transition temperature (T_{trans}) in the subsequent shape memory process.

3.5. Cross-link density analysis

Cross-linking provides the necessary fixing elements for shape memory during deformation. PA11 is physically cross-linked with PUA, and the cross-linking density was calculated using the Flory-Rehner equation [23]. The physical cross-linking point can be used as the stationary phase to improve the fixation and recovery rates. Simultaneously, energy was stored inside the material to promote shape recovery and release stress, making it easier for the material to return to its original shape. Therefore, a higher degree of cross-linking contributes to an improved recovery rate.

The filming process compounded the two materials, followed by hot pressing. The spinning process

Table 1. Glass transition temperature of PA11, PUA, the PA11/PUA film, and PA11/PUA fiber.

Sample	T_g of soft segment PU [°C]	T_g of hard segment PU [°C]	γ -relaxation PA11 [°C]	β -relaxation PA11 [°C]	α -relaxation PA11 [°C]
PA11	–	–	-80	7	53
PUA	-87	-12	–	–	–
PA11/PUA film	-72	-28	–	17	–
PA11/PUA fiber	–	-20	–	48	–

Table 2. Cross-linking density of the PA11/PUA fiber.

Sample	m_1 [g]	m_2 [g]	Q	Cross-link density, ν [mol/cm ³]
PA11/PUA film	0.0160	0.0168	0.050	36.9
PA11/PUA fiber	0.1240	0.1360	0.096	12.4

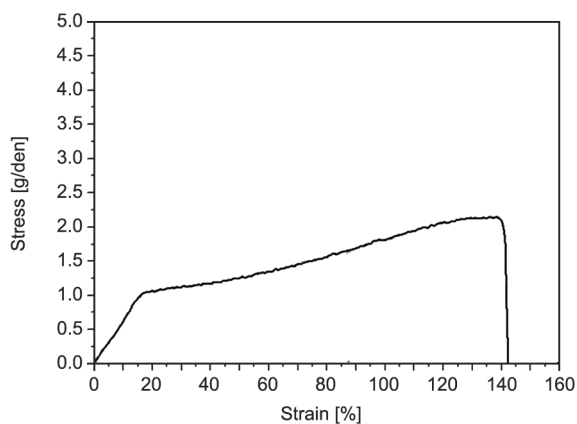


Figure 8. Tensile test for PA11/PUA sea-island fiber. The results show that the tensile strength is low, presumably owing to over-cross-linking between PA11 and PUA fiber.

Table 3. Tensile test data for PA11/PUA sea-island fiber.

Sample	Fineness [den]	Strength [g/den]	Strain [%]
PA11/PUA fiber	7.5	2.42±0.15	142.91±8.43

requires cross-linking of the two materials after a brief encounter in the die, followed by rapid cooling into filaments. Therefore, as shown in Table 2, the cross-linking density of the film was significantly higher than that of the fibers.

3.6. Fiber characteristics

The results of the spun fiber tensile tests are shown in Figure 8. The spun fiber was tested to be 7.5 den, and the relevant data are summarized in Table 3. The results show that the tensile strength is low, presumably due to over-cross-linking between the PA11 and PUA fibers, resulting in a decrease in strength.

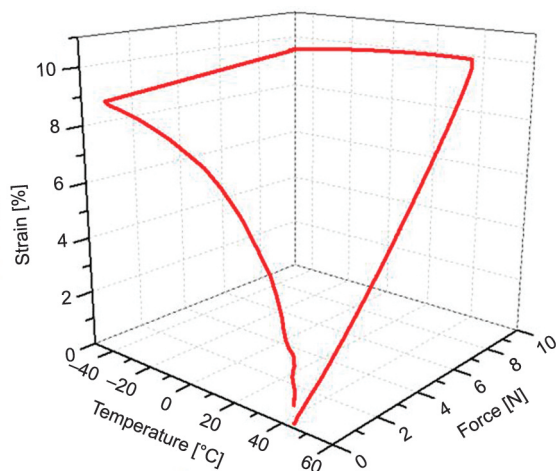


Figure 9. Shape memory test curve of PA11/PUA film. The test results show that PA11/PUA has excellent shape memory fixation and recovery rates.

3.7. Shape memory behavior

First, the shape memory performance of the film was used to determine whether it could feasibly be used to fabricate melt-spun fibers. The shape memory fixation and recovery rates of the PA11/PUA film test pieces are listed in Table 4. The shape memory curves are shown in Figure 9. Table 4 shows that the shape memory fixation rate of the PA11/PUA film was 99.6% and the recovery rate was 92.3%, proving that PA11/PUA had good shape memory fixation and recovery rates. Melt-spinning was performed to test the shape memory effect of the fibers.

The PA11/TPU sea-island composite fibers were prepared using a bicomponent melt-spinning machine with a sea-island-type spinning nozzle. PA11 was used as the sea component, and PUA was used as the island component. Figure 10 shows that different fibers have obvious interfaces between the two phases of the single-fiber cross-section, demonstrating the fabrication of the composite fibers was successful.

The shape memory effect of the PA11/PUA island fibers was evaluated. Three-dimensional (3D) curves are shown in Figure 9. The fixation and recovery rates for the three cycles were calculated. The quantitative data are presented in Table 5.

Table 4. Shape memory fix, recovery rate of PA11/PUA film.

Sample	R_f [%]	R_r [%]
PA11/PUA film	99.6	92.3

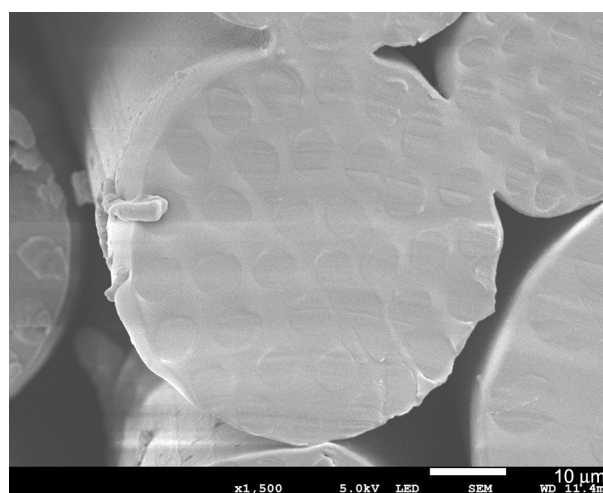


Figure 10. SEM image of the cross-section of PA11/PUA single fiber. PA11 as the component of the sea and PUA as the component of the island. It shows a clear interface between the PA11/PUA and forming a sea-island structure.

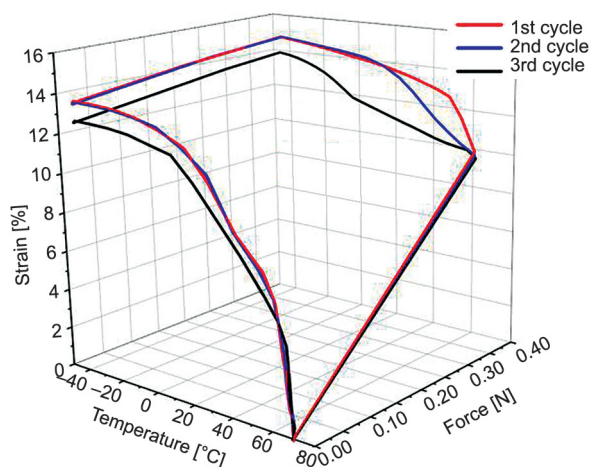


Figure 11. PA11/PUA fiber three cycles shape memory curve. There is continuous stretching after reaching the relative stress of the deformation, and finally, it releases the stress and cools down to complete the shape memory cycle.

Table 5. Shape memory fix, recovery rate of PA11/PUA fiber.

Sample	R_f [%]	R_r [%]
1 st cycle	98.8	99.9
2 nd cycle	98.8	99.2
3 rd cycle	98.8	99.9

From Figure 11, it can be observed that when the PA11/PUA fiber is subjected to the same application of 0.65 N at 68 °C to achieve a deformation of 10%, the deformation remains stable after three cycles. There is continuous stretching after reaching the relative stress of the deformation, and finally release the stress and cool down to complete the shape memory cycle.

The PA11/PUA fibers exhibited excellent shape memory fixation and recovery rates. The fiber maintained its shape during the three cooling cycles and its length was maintained without significant shrinkage after the stress was released. No relaxation or contraction occurred during the three cycles of heating and application of the same stress. This is because PUA and PA11 have better compatibility between the two phases and are more stable during the shape memory process.

3.8. Constrained recovery

A detailed analysis of the shape recovery mechanism was conducted. The specimen was cooled after the application of strain, the molecular segments stopped moving, and energy was stored inside the specimen.

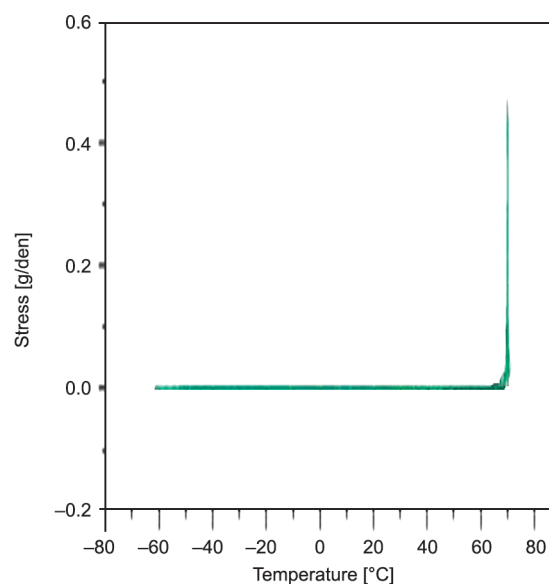


Figure 12. Constrained recovery of PA11/PUA fiber. The shape recovery process of these fibers is relatively gentle and does not generate excessive stress.

Table 6. Constrained recovery data of PA11/PUA fiber.

	Recovery strength [g/den]	Relative temperature [°C]	T_{trans} [°C]
PA11/PUA	0.6	68	68

This stored internal strain energy is easily released after heating and can be presented as a force. This is called constrained recovery stress, which is the force that recovers the deformation of the test piece during the heating process from fix temperature (T_{fix}) to transition temperature (T_{trans}) under a set strain. In general, the recovery stress emerges from both the internal strain-stored energy and the configurational state entropy. The high internal strain-stored energy and low configurational state entropy can be easily relieved by heating to recover the original shape [30]. The test results for the spun fibers are shown in Figure 12, where the stress reaches a maximum value near T_{trans} . The recovery stress decreased further with increasing temperature because most of the molecular chains were disoriented above this temperature range. Table 6 presents the maximum constrained recovery strength of the PA11/PUA fibers and a comparison between the temperature and T_{trans} of the constrained recovery stress. This could have been caused by the difference in fiber strength in the previous test, resulting in a difference in the mechanical properties between the two in subsequent applications.

4. Conclusions

In this study, we first evaluated the compatibility of PA11/PUA blend systems with the shape memory performance of the films. The results showed that the PA11/PUA blend system's two-phase compatibility was better and had a co-continuous phase. After one shape memory session, the fixation rate of the PA11/PUA film was 99.6%, the recovery rate was 92.4%, and the shape memory performance was satisfactory.

After evaluating the PUA systems through the film, PA11/PUA composite fibers were successfully prepared by melt-spinning. After three shape memory cycles, the PA11/PUA fiber fixation and recovery rates were 98.8%, and the recovery rate was 99.9%. Compared with the film, the recovery rate was improved because, during the fiber spinning process, the material was subjected to a tensile force along the direction, which increased the degree of conformity. The PA11/PUA composite fibers exhibited a two-phase structure at the contact interface. This is the ideal fiber in terms of capacitance, and is the most stable among the three memory shapes. There was no increase in fiber toughness or relaxation. Because the strain energy of the sea island structure is more dispersed, the shape-recovery process of this type of fiber is gentle and does not generate excessive stress. Therefore, this structure can reduce the stress concentration effect and smooth the shape recovery process, making it suitable for high-durability shape memory materials.

The scalability of PA11/TPU shape memory sea island fibers presents a transformative opportunity across multiple industries. Their ability to combine functional adaptability, high durability, and lightweight characteristics make them ideal for next-generation applications in smart textiles, biomedical engineering, aerospace, and consumer electronics [31, 32]. Future research should focus on process optimization, cost-effective synthesis, and multifunctional integration to fully realize commercial potential.

References

- [1] Xia Y., He Y., Zhang F., Liu Y., Leng J.: A review of shape memory polymers and composites: Mechanisms, materials, and applications. *Advanced Materials*, **33**, 2000713 (2021).
<https://doi.org/10.1002/adma.202000713>
- [2] Qi X., Dong Y., Zahidul Islam M. D., Zhu Y., Fu Y., Fu S-Y.: Excellent triple-shape memory effect and superior recovery stress of ethylene-vinyl acetate copolymer fiber. *Composites Science Technology*, **203**, 108609 (2021).
<https://doi.org/10.1016/j.compscitech.2020.108609>
- [3] Budun S., İsgören E., Erdem R., Yüksek M.: Morphological and mechanical analysis of electrospun shape memory polymer fibers. *Applied Surface Science*, **380**, 294–300 (2016).
<https://doi.org/10.1016/j.apsusc.2015.12.235>
- [4] Sharafi S., Li G.: Multiscale modeling of vibration damping response of shape memory polymer fibers. *Composites Part B*, **91**, 306–314 (2016).
<https://doi.org/10.1016/j.compositesb.2015.12.046>
- [5] Shirole A., Sapkota J., Foster E. J., Weder C.: Shape memory composites based on electrospun poly(vinyl alcohol) fibers and a thermoplastic polyether block amide elastomer. *ACS Applied Materials and Interfaces*, **8**, 6701–6708 (2016).
<https://doi.org/10.1021/acsami.6b00834>
- [6] Liu R., Kuang X., Deng J., Wang Y-C., Wang A. C., Ding W., Lai Y-C., Chen J., Wang P., Lin Z., Qi H. J., Sun B., Wang Z. L.: Shape memory polymers for body motion energy harvesting and self-powered mechanosensing. *Advanced Materials*, **30**, 1705195 (2018).
<https://doi.org/10.1002/adma.201705195>
- [7] Xie T.: Tunable polymer multi-shape memory effect. *Nature*, **464**, 267–270 (2010).
<https://doi.org/10.1038/nature08863>
- [8] Zotzmann J., Behl M., Hofmann D., Lendlein A.: Reversible triple-shape effect of polymer networks containing poly(pentadecalactone)- and poly(ϵ -caprolactone)-segments. *Advanced Materials*, **22**, 3424–3429 (2010).
<https://doi.org/10.1002/adma.200904202>
- [9] Bai Y., Zang X., Wang Q., Wang T.: A tough shape memory polymer with triple-shape memory and two-way shape memory properties. *Journal of Materials Chemistry A*, **2**, 4771–4778 (2014).
<https://doi.org/10.1039/c3ta15117d>
- [10] Sun L., Huang W. M.: Mechanisms of the multi-shape memory effect and temperature memory effect in shape memory polymers. *Soft Matter*, **6**, 4403–4406 (2010).
<https://doi.org/10.1039/c0sm00236d>
- [11] Dong Y., Xia H., Zhu Y., Ni Q-Q., Fu Y.: Effect of epoxy-graft-polyoxyethylene octyl phenyl ether on preparation, mechanical properties and triple-shape memory effect of carbon nanotube/water-borne epoxy nanocomposites. *Composites Science Technology*, **120**, 17–25 (2015).
<https://doi.org/10.1016/j.compscitech.2015.09.011>
- [12] Stoclet G., Seguela R., Lefebvre J-M: Morphology, thermal behavior and mechanical properties of binary blends of compatible biosourced polymers: Poly(lactide)/polyamide11. *Polymer*, **52**, 1417–1425 (2011).
<https://doi.org/10.1016/j.polymer.2011.02.002>

- [13] Nuzzo A., Coiai S., Carroccio S. C., Dintcheva N. T., Gambarotti C., Filippone G.: Heat-resistant fully bio-based nanocomposite blends based on poly(lactic acid). *Macromolecular Materials Engineering*, **299**, 31–40 (2014).
<https://doi.org/10.1002/mame.201300051>
- [14] Reulier M., Avérous L.: Elaboration, morphology and properties of renewable thermoplastics blends, based on polyamide and polyurethane synthesized from dimer fatty acids. *European Polymer Journal*, **67**, 418–427 (2015).
<https://doi.org/10.1016/j.eurpolymj.2014.11.036>
- [15] Zhang S-L., Wang G-B., Jiang Z-H., Wang D., Ma R-T., Wu Z-W.: Impact properties, phase structure, compatibility, and fracture morphology of polyamide-1010/thermoplastic poly(ester urethane) elastomer blends. *Journal of Polymer Science: Part B: Polymer Physics*, **43**, 1177–1185 (2005).
<https://doi.org/10.1002/polb.20410>
- [16] Zhang S-L., Wang D., Guan S-W., Jiang Z-H., Wu Z-W., Wang G-B.: Toughening mechanism of PA1010/ester-based TPU blends. *Materials Letters*, **61**, 267–273 (2007).
<https://doi.org/10.1016/j.matlet.2006.04.050>
- [17] Genovese A., Shanks R. A.: Simulation of the specific interactions between polyamide-6 and a thermoplastic polyurethane. *Computational and Theoretical Polymer Science*, **11**, 57–62 (2001).
[https://doi.org/10.1016/S1089-3156\(99\)00059-8](https://doi.org/10.1016/S1089-3156(99)00059-8)
- [18] Chiu F-C., Lai S-M., Chen Y-L., Lee T-H.: Investigation on the polyamide 6/organoclay nanocomposites with or without a maleated polyolefin elastomer as a toughener. *Polymer*, **46**, 11600–11609 (2005).
<https://doi.org/10.1016/j.polymer.2005.09.077>
- [19] Chiu H-T., Chuang C-Y.: The mechanical and rheological behavior of the PA/TPU blend with POE-g-MA modifier. *Journal of Applied Polymer Science*, **115**, 1278–1282 (2010).
<https://doi.org/10.1002/app.30944>
- [20] Rashmi B. J., Loux C., Prashantha K.: Bio-based thermoplastic polyurethane and polyamide 11 bioalloys with excellent shape memory behavior. *Journal of Applied Polymer Science*, **134**, 44794 (2017).
<https://doi.org/10.1002/app.44794>
- [21] Hwang W-G., Wei K-H., Wu C-M.: Mechanical, thermal, and barrier properties of NBR/organosilicate nanocomposites. *Polymer Engineering and Science*, **44**, 2117–2124 (2004).
<https://doi.org/10.1002/pen.20217>
- [22] Czifrák K., Karger-Kocsis J., Daróczy L., Zsuga M., Kéki S.: Poly(ϵ -caprolactone) and pluronic diol-containing segmented polyurethanes for shape memory performance. *Macromolecular Chemistry and Physics*, **215**, 1896–1907 (2014).
<https://doi.org/10.1002/macp.201400237>
- [23] Sperling L. H.: Introduction to physical polymer science. Wiley, Hoboken (1993).
- [24] Zhao Q., Zou W., Luo Y., Xie T.: Shape memory polymer network with thermally distinct elasticity and plasticity. *Science Advances*, **2**, e1501297 (2016).
<https://doi.org/10.1126/sciadv.1501297>
- [25] Hu J. L., Ji F. L., Wong Y. W.: Dependency of the shape memory properties of a polyurethane upon thermomechanical cyclic conditions. *Polymer international*, **54**, 600–605 (2005).
<https://doi.org/10.1002/pi.1745>
- [26] Rashmi B. J., Rusu D., Prashantha K., Lacrampe M-F., Krawczak P.: Development of bio-based thermoplastic polyurethanes formulations using corn-derived chain extender for reactive rotational molding. *Express Polymer Letters*, **7**, 852–862 (2013).
<https://doi.org/10.3144/expresspolymlett.2013.82>
- [27] Li W. L., Liu J. L., Hao C. W., Jiang K., Xu D. F., Wang D. J.: Interaction of thermoplastic polyurethane with polyamide 1212 and its influence on the thermal and mechanical properties of TPU/PA1212 blends. *Polymer Engineering and Science*, **48**, 249 (2008).
<https://doi.org/10.1002/pen.20853>
- [28] López-Barrón C. R., Macosko C. W.: Rheological and morphological study of cocontinuous polymer blends during coarsening. *Journal of Rheology*, **56**, 1315–1334 (2012).
<https://doi.org/10.1122/1.4739067>
- [29] Martino L., Basilissi L., Farina H., Ortenzi M. A., Zini E., di Silvestro G., Scandola M.: Bio-based polyamide 11: Synthesis, rheology and solid-state properties of star structures. *European Polymer Journal*, **59**, 69–77 (2014).
<https://doi.org/10.1016/j.eurpolymj.2014.07.012>
- [30] Small W., Singhal P., Wilson T. S., Maitland D. J.: Bio-medical applications of thermally activated shape memory polymers. *Journal of Materials Chemistry*, **20**, 3356–3366 (2010).
<https://doi.org/10.1039/B923717H>
- [31] Thakur S.: Shape memory polymers for smart textile applications. in ‘Textiles for advanced applications’ (eds.: Kumar B., Thakur S.) IntechOpen, Delhi, 323–337 (2017).
<https://doi.org/10.5772/intechopen.69742>
- [32] Wang L., Zhang F., Liu Y., Leng J.: Shape memory polymer fibers: Materials, structures, and applications. *Advanced Fiber Materials*, **4**, 5–23 (2022).
<https://doi.org/10.1007/s42765-021-00073-z>